Ordered Local Domain Structures of Decaneselenolate and Dodecaneselenolate Monolayers on Au{111}

Jason D. Monnell,[†] Joshua J. Stapleton,[‡] Jennifer J. Jackiw,[†] Tim Dunbar,[‡] William A. Reinerth,[§] Shawn M. Dirk,[§] James M. Tour,*[,§] David L. Allara,*[,‡] and Paul S. Weiss*[,†]

Departments of Chemistry, Physics, and Materials Science, 104 Davey Laboratory, The Pennsylvania State University, University Park, Pennsylvania 16802-6300, and Department of Chemistry and Center for Nanoscale Science and Technology, Rice University, Houston, Texas 77005

Received: December 5, 2003; In Final Form: February 29, 2004

Coexisting adsorbate phases in high-coverage decaneselenolate and dodecaneselenolate [$CH_3(CH_2)_nSe$, n = 9 and 11] self-assembled monolayers on Au{111} have been characterized by scanning tunneling microscopy and consist of two types: a densely packed distorted hexagonal lattice incommensurate to the underlying gold substrate, as revealed by the observation of a moiré pattern, and a commensurate linear missing-row structure. Examination of the nearest neighbor distances in the tightly packed lattice reveal two distinct repeat distances of 4.90 and 5.20 Å, which complements previous surface X-ray data. The linear missing row structure manifests in several variants of the $(\sqrt{3} \times 3\sqrt{3})$R30° unit cell differentiated by whether the molecules bind at 2- or 3-fold substrate sites. While the number of molecules within this unit cell is typically two, in some cases an additional alkaneselenolate molecule is located at a site one Au atom lower than the rest. The structural conclusions are supported by excellent agreement of experimental lattice parameters and those derived from molecular packing models. Comparison of the alkaneselenolate data with analogous structural phases reported for alkanethiolate monolayers on Au{111} shows that differences between the two systems can be understood on the basis that self-assembly is guided both by headgroup−headgroup as well as headgroup−substrate interactions.

Introduction

At present, much of our knowledge of the structure, formation, stability, and dynamics of self-assembled monolayers (SAMs), relevant to nanoscale applications, is based on reports of *n*-alkanethiolates on Au{111}.[1−17] These studies show that different characteristic surface morphologies and electronic properties of monolayers can result from changes in the molecular structure and assembly conditions. It is generally understood that the balance between headgroup−substrate and intermolecular interactions is of critical importance for the overall molecular surface structure and coverage, whereas the polar and steric character of the tailgroup determines the final ambient interface arrangement in the SAM.[18−24] While interactions between different alkyl tail chains are beginning to be understood, the characteristics contributed by the headgroup, i.e. the atoms that attach the alkyl chain to the surface, have not been as well characterized. Thus, in order for self-assembly to become a more broadly useful tool, variations in the headgroup attachment need to be explored and coupled with detailed characterization to develop fundamental correlations with SAM structure. In particular, for gold surfaces, modes of attachment need to be extended from the S−Au bonds to other chemically suitable combinations, including isonitrile (−NC)[25−29] and other chalcogenides, such as Se and Te.[30,31] By exploring both headgroups and exposed interface structures, the contributions of all the molecular components to the monolayer structure and stability can be understood, enabling more flexible designs for applications.

The chalcogens in their divalent oxidation state are natural choices for the substrate linker group, since they exhibit highly polarizable outer electrons that can lead to strong donor−acceptor bonding with polarizable (soft) metals. Recently, interest has arisen in both the electronic and structural nature of alkyl monolayers bound to the Au{111} surface with Se atoms.[13,31−45] Relevant to electronic applications, significant differences in the conductance characteristics between S- and Se-based SAMs have been reported. On the basis of theoretical calculations of the differences between the valence and conduction energies, Ratner and co-workers concluded that α,α′-xylyldiselenol molecules assembled on Au should conduct 25 times better than the equivalent dithiols and 75 times better than those with hydroxyl termini.[43] In support of such differences, Gauthier and co-workers concluded from scanning tunneling microscopy (STM) experiments that Se termination provides better electronic coupling to Au than the S headgroup for bischalcogen-terthiophene.[33] Given these significant differences in the headgroup-Au electronic states, one might expect corresponding differences in the binding and geometric arrangements the headgroups for similar types of SAMs. Limited studies support this conclusion. Huang et al. conducted surface-enhanced Raman spectroscopy measurements and concluded that selenol molecules adsorb to gold more readily and likely pack

* To whom correspondence should be addressed. E-mail (P.S.W.): stm@psu.edu.

[†] Departments of Chemistry and Physics, The Pennsylvania State University.

[‡] Departments of Chemistry and Materials Science, The Pennsylvania State University.

[§] Department of Chemistry and Center for Nanoscale Science and Technology, Rice University.

10.1021/jp037728x CCC: $27.50
Published on Web 06/22/2004

at lower densities than the equivalent thiolates.[41] Feher and coworkers reported that diphenylselenolate and benzeneselenolate deposited on Au{111} SAMs yield qualitatively similar ($3\sqrt{3} \times 2\sqrt{3}$)R30° structures and both reconstruct the Au substrate to form large hexagonal islands. However, molecular resolution images of these monolayers were not attained; thus, the assignment of the structure and number of molecules within the unit cell were not certain.[39] The most detailed structural data come from surface X-ray diffraction data, which show that a fully formed docosaneselenol SAM on Au{111} exhibits an incommensurate structure with a 4.897 Å × 5.204 Å, $\gamma = 120°$ unit cell,[37] noticeably different than the primary ($\sqrt{3} \times \sqrt{3}$)-R30° unit cell and its superlattices, reported for a fully formed alkanethiolate SAM.[5,7,8,10,14,16,46−50,51]

On the basis of the rich variety of morphologies reported for the well-studied family of alkanethiolate on Au{111} SAMs, one would expect an analogous situation in alkaneselenolate SAMs, with potential structural differences arising from changes in headgroup−substrate interactions. Given the limited data available for the alkaneselenolate case, we have explored structural variations in alkaneselenolate on Au{111} SAMs with the idea of building correlations with headgroup−substrate, headgroup−headgroup, and molecule (tail)−molecule interactions, as well as utilizing the data in further studies of the electronic characteristics of molecules ordered in SAMs. Of particular interest in this report are STM studies of structural phases on high-coverage surfaces. Our data reveal two major structural regimes: one a phase with densely packed adsorbates arranged incommensurately to the Au substrate and the other a series of phases with incomplete coverage exhibiting missing row structures. Through comparisons with packing models, both structures show variability in the binding site involving both bridge and 3-fold hollow sites. Analysis of these data and comparisons with analogous alkanethiolate SAMs indicates that headgroup−headgroup as well as headgroup−substrate interactions are critical in guiding self-assembly.

Experimental Section

Decaneselenolate and dodecaneselenolate SAMs were prepared on freshly hydrogen flame annealed mica supported Au{111} substrates (Molecular Imaging Inc., Phoenix, AZ) from 0.3 and 0.2 mM didecane diselenide and didodecane diselenide solution, respectively, in freshly distilled (Na/benzophenone) THF, in a N_2-purged atmosphere in a glovebox for 21 h. The two dialkyl diselenides were prepared according to known protocols.[52,53]

All STM experiments were performed under ambient conditions, at sample biases of ±1.0 V and tunneling currents between 1.0 and 3.0 pA, using custom-built instrumentation described previously.[1] Images were calibrated by comparison to images of decanethiolate films taken immediately prior to these experiments. The surface structures are quite stable in an ambient environment for several months, although some motion can be observed in which the missing row structures tend to coalesce to the dense form over time. Modeling of the observed images of the surface, including moiré patterns, was done through the superposition of two lattices, as suggested by Rong and Kupier's, and Yamamoto et al.'s model of the moiré patterns on graphite, Terada et al.'s model of Pd on Ni{111}, and Parkinson et al.'s model of transition-metal dichalcogenides.[54−57] For the substrate lattice model, Au atoms were hexagonally arranged at the standard 2.884 Å interatomic distance between centers of atoms, although substrate relaxation most likely occurs in these and other related systems. In the model for the missing row structure, selenolate molecules were placed in 3-fold hollow and bridge binding sites, filling these sites to match our observations. For the incommensurate structure, the selenolate adlayer unit cell was created using the dimensions published by Samant obtained using surface X-ray diffraction (unit cell: $a = 5.204$ Å, $b = 4.897$ Å, and $\gamma = 120°$).[37] Since similar observations were obtained from both decaneselenolate and dodecaneselenolate films, images that best illustrate the observed structures were selected for each set of results. The raw data are shown as topographic maps without any filtering or processing.

Results and Discussion

Sample Morphology. A number of samples, prepared identically and designed to give saturated monolayer coverage, were examined. In each case the STM measurements revealed the coexistence of several distinct structural phases of the film. Typical regions showing disorder were observed, but the majority of surfaces exhibited domains with densely packed structures and domains with missing row structures formed at incomplete coverage. The surface morphologies were found to be stable with storage under ambient conditions, but conversion of an incomplete coverage structure to a densely packed one has been observed. We first discuss the densely packed structure, which we infer is the maximum coverage monolayer phase. The incomplete coverage, missing row structures are then presented. Finally, we discuss the mechanisms of monolayer growth and use comparisons with data reported for alkanethiolate/Au{111} SAMs to consider the role of headgroup interactions in controlling the surface structures in alkaneselenolate and alkanethiolate SAMs.

The Densely Packed Incommensurate Monolayer Structure−Observation of Moiré Patterns. The simplest structure we observed for selenolate adsorbates on the Au{111} surface is the densely packed incommensurate monolayer. This structure produces a moiré pattern in STM images, indicating there is a lattice mismatch in which selenolate molecules reside on sites not necessarily in registry with the surface or bulk atoms of the underlying Au lattice.[58] Figures 1, 2, and 3a show images of dodecaneselenolate monolayers exhibiting these moiré patterns over many unit cells. In Figure 1, note the substrate vacancy islands, which appear as depressions in the vicinity of the domain boundaries of the gold islands (protrusions) and can be ascribed to Au atom vacancies. Both the Au substrate vacancies and domain boundary defects are present at much smaller densities than typically observed in most thiol-terminated SAMs,[10] where they are common features spaced at the nanometer scale. Note the complete absence of vacancy islands in Figure 2. Given the relative reduction in defect densities in alkaneselenolate compared to alkanethiolate SAMs for similar methods of preparation (e.g., room temperature), we conclude that surface mobility and reconstruction processes (e.g., via Ostwald ripening),[9,49] which underlie the dynamics of the coalescence of these defects, are more accessible for alkaneselenolate monolayers.

The unit cell dimensions (~4.90 Å and ~5.20 Å, $\gamma = \sim 120°$) observed in the higher resolution images (Figures 3a and 4) match those reported from surface X-ray diffraction.[37] A graphical model was created using the surface X-ray diffraction dimensions repeated over a large scale and overlaid on an unreconstructed Au{111} lattice. The match of the resulting moiré pattern (Figure 3b) with the one observed in the STM image (Figure 3a) indicates that the model can describe the observed data. This type of model, however, explores solely

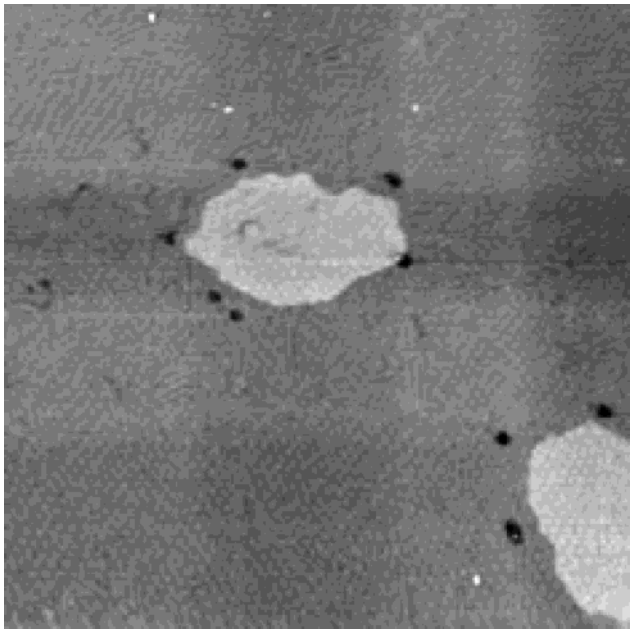

Figure 1. STM image of a 2200 Å × 2200 Å area of a dense-packed region of a decaneselenolate on Au{111} SAM recorded at +1.0 V sample bias and 3.0 pA tunneling current. The large protruding areas in the center and lower right-hand corner are Au islands covered with a decaneselenolate monolayer and the smaller depressions surrounding them are Au vacancy defects. The latter features are commonly found at high surface densities in alkanethiolate systems, but note how they are located sparsely and only adjacent to Au islands in densely packed regions of alkaneselenolate SAMs. These enhanced islands and vacancies commonly occur from Ostwald ripening of the surface during and after monolayer deposition and serve as a supply and sink for atoms for surface reconstruction. The uniform pattern of small dots distributed over the entire surface, including the gold islands, is a moiré pattern that arises from the registry of the SAM molecules on the gold lattice.

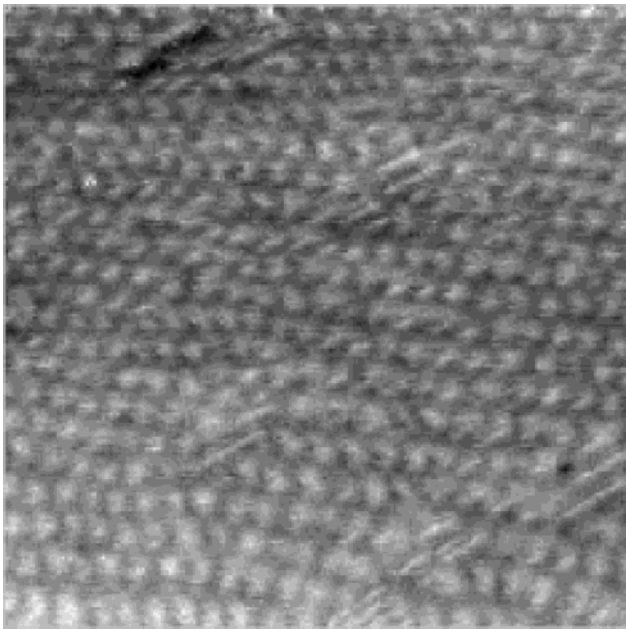

Figure 2. STM image of a 800 Å × 800 Å area of a dense-packed region of a dodecaneselenolate on Au{111} SAM recorded at +1.0 V sample bias and 3.0 pA tunneling current. This image shows the moiré pattern distributed over the surface of the film as well as some of the linear row structures of the adsorbate molecules. Notice the absence of gold vacancy islands (refer to Figure 1).

the lattice mismatch between the adsorbate and substrate and thus does not predict the STM intensity patterns, which also include electronic interactions between the Au and selenolate molecules. Further calculations could determine the electronic interactions.[55,59,60] The moiré period obtained by Fourier analysis of images similar to that shown in Figure 3a reveals peaks at 34 and 52 Å, within 1% of the proposed models. These periods contain ca. seven and 10 repeats of the 4.90 and 5.20 Å unit cell lengths, respectively. This comparison serves as an internal calibration of the moiré pattern and distances measured by STM.

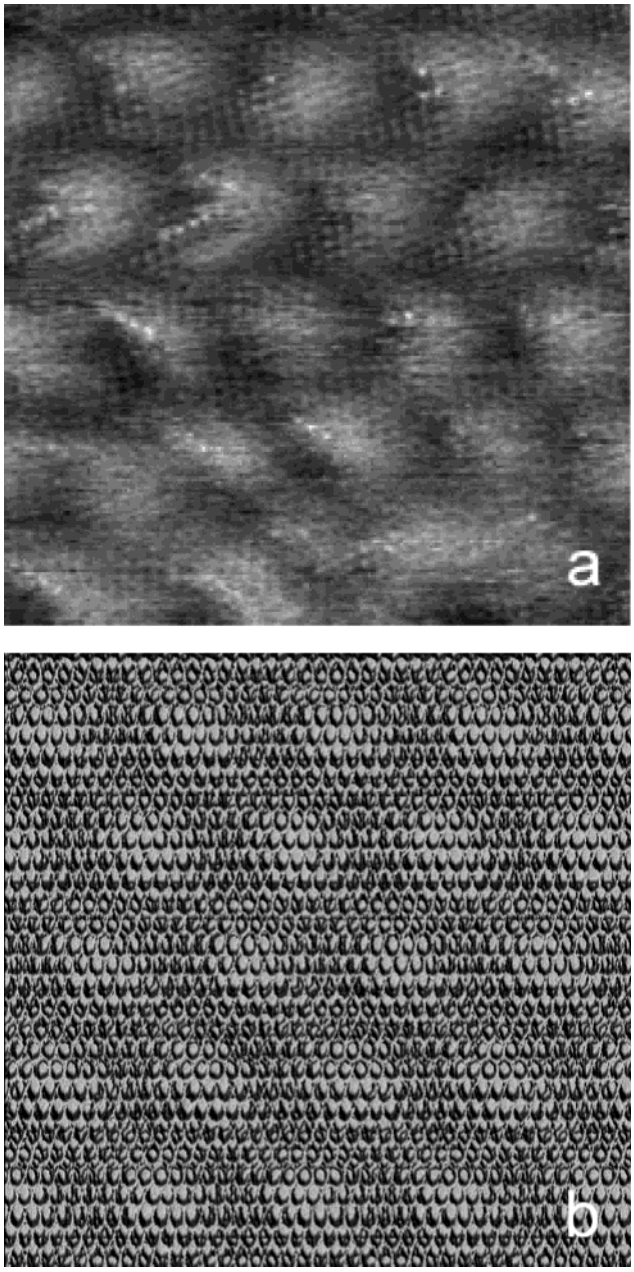

Figure 3. (a) STM image of a 165 Å × 165 Å area of a dense-packed region of a dodecaneselenolate on Au{111} SAM recorded at +1.0 V sample bias and 3.0 pA tunneling current. This image shows molecular resolution of the monolayer, seen as the smallest light spots, as well as the moiré pattern, seen as the larger spots. (b) Model of a 165 Å × 165 Å area of an *n*-alkaneselenolate dense-packed region on an unreconstructed Au{111} surface based on the unit cell determined by X-ray diffraction.[51]

We observed that the moiré pattern repeats at intervals similar to that expected for "buckling" of the surface expected from the (22 × $\sqrt{3}$) reconstruction of the bare gold surface.[49,61,62] These moiré patterns, visible in Figures 2 and 3, may arise from a "nodal network array" formed by an adsorbate-induced surface

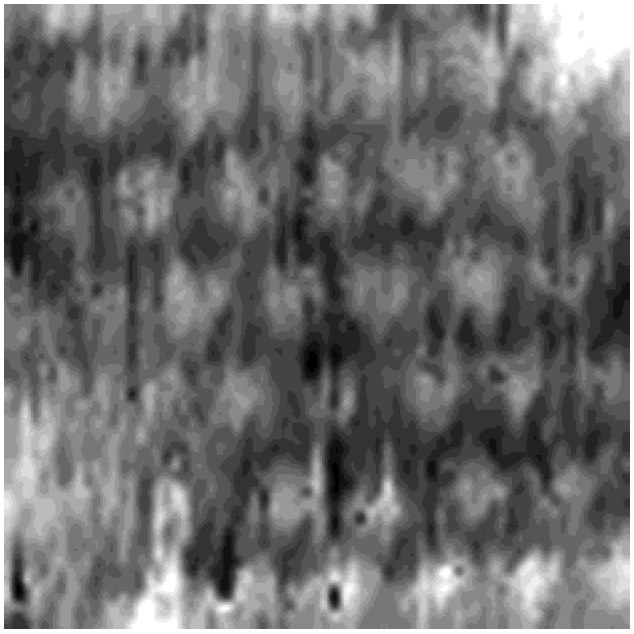

Figure 4. STM image of a 34 Å × 34 Å area of a dense-packed region of a dodecaneselenolate on Au{111} SAM recorded at a sample bias of +1.0 V and 3 pA tunneling current. The image shows the molecular arrangement in detail. Analysis of many of these structures yields a unit cell with 5.20 Å × 4.90 Å lattice constants.

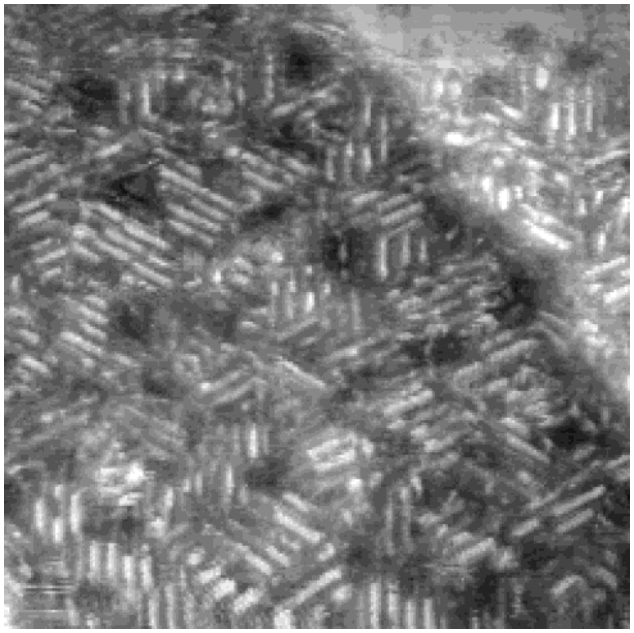

Figure 5. STM image of a 440 Å × 440 Å area of an incomplete coverage region of a dodecaneselenolate on Au{111} SAM recorded at a sample bias of +1.0 V and a tunneling current of 3.0 pA. The image shows the distribution of linear missing row structures over the surface.

reconstruction of the native herringbone reconstruction of the Au{111} surface.[63] This nodal network would relieve the surface stress of the herringbone reconstruction, while allowing the adsorbate−surface to reconstruct and thus absorb previously existing surface point defects or adatoms as well as adsorbate-induced defects (vacancy islands and domain features), as seen in Figures 5 and 6. Ag on Pt{111} forms a trigonal nodal network array with a period of 44.8 Å ± 1.4 Å containing eight or nine atoms per beat.[64] This is comparable to the periods of seven and 10 molecules we observe between each moiré node here.

Incomplete Coverage Regions—Missing Row Structures. There have been reports of missing row structures found in incomplete monolayers of alkanethiolates on Au{111}, explained either on the basis of dimerized adsorbates[65] or binding to substrate lattice sites in an $(m\sqrt{3} \times n\sqrt{3})R30°$ overlayer structure.[5,9,10,16,17,48] Our images of the selenolate analogues also show missing row structures. Specifically, the selenolate rows are rotated 30° and run along the $[1\bar{2}1]$ direction relative to the Au{111} substrate.[5,8,16] Decaneselenolate and dodecaneselenolate moieties have several variants, with lattice spacings of 4.99 Å × 14.69 Å, 14.99 Å = $3\sqrt{3}$ Au lattice spacings, 15.26 Å, and 15.60 Å, as determined by Fourier analysis of many images. These variants can be explained by having the Se headgroups shift back and forth between adjacent Au bridge and 3-fold lattice sites. Figures 5 and 6a show primarily the 4.99 Å × 15.60 Å variant of the $(\sqrt{3} \times 3\sqrt{3})R30°$ missing row configuration in a dodecaneselenolate monolayer surface. Figure 6b is a diagram of variability among these binding sites. Analysis of these potential binding sites relative to both a surface featuring a herringbone reconstruction and an unreconstructed underlying Au{111} lattice reveals that binding sites consist of bridge positions and both the fcc and hcp 3-fold sites.

Each of the $(\sqrt{3} \times 3\sqrt{3})R30°$ unit cell variants are comprised of multiples of fundamental unit cells. Densely packed phase unit cells are common, with the 15.60 Å variant comprised of three units of the 5.20 Å unit length, while the 14.69 Å variant has three units of the 4.90 Å unit length. Other fundamental units are also observed: the 14.99 Å variant contains three $\sqrt{3}$ Au lattice spacings and the 15.26 Å length is a distance from a 3-fold site to a 3-fold or bridge site (or between any like sites). The model presented in Figure 6b shows these different spacings as black dots lying on the colored arcs. By shifting the binding, the model represents reconstructed areas (15.60 and 14.69 Å), areas where the reconstruction has been lifted (14.99 Å), or transition areas (15.26 Å). These observations of different characteristic spacings indicate that for incomplete monolayers, alkaneselenolates reside on a mixture of reconstructed and unreconstructed Au substrate features on fcc and hcp 3-fold and bridge sites.

With less than full monolayer coverage, fcc and hcp 3-fold as well as bridge sites are available for individual molecules to adsorb. This is evident by the even distribution of the variant structures in the data. In addition, molecules that appear to be ~2 Å below the height of the others in our constant current images are found between the missing rows (Figure 6c) and, when put into context of the model, are inferred to occupy bridge and 3-fold sites. A line profile (Figure 6d) shows the apparent height difference between the prominent double row and the molecules in the "missing row" and the distance distribution of these molecules. Adsorbate surface mobility, as well as variability in binding sites, has been observed in thiolates (discussed further in the following section); theoretical calculations of the differences in energies between these various sites suggest that binding occurs at a combination of bridge and hcp and fcc 3-fold locations.[47,66] Given the similarity between S and Se, one might expect that selenolates would also exhibit this behavior.

Intermediate States in Monolayer Growth—Differences between Alkaneselenolates and Alkanethiolates. The differences between the lower and higher coverage structures suggest intermediate steps in the growth of alkaneselenolate SAMs on Au{111}. This picture can be augmented by comparisons with the extensive details reported on the formation of analogous alkanethiolate SAMs, which reveal important differences between the S and Se cases. Poirier has observed the evolution of

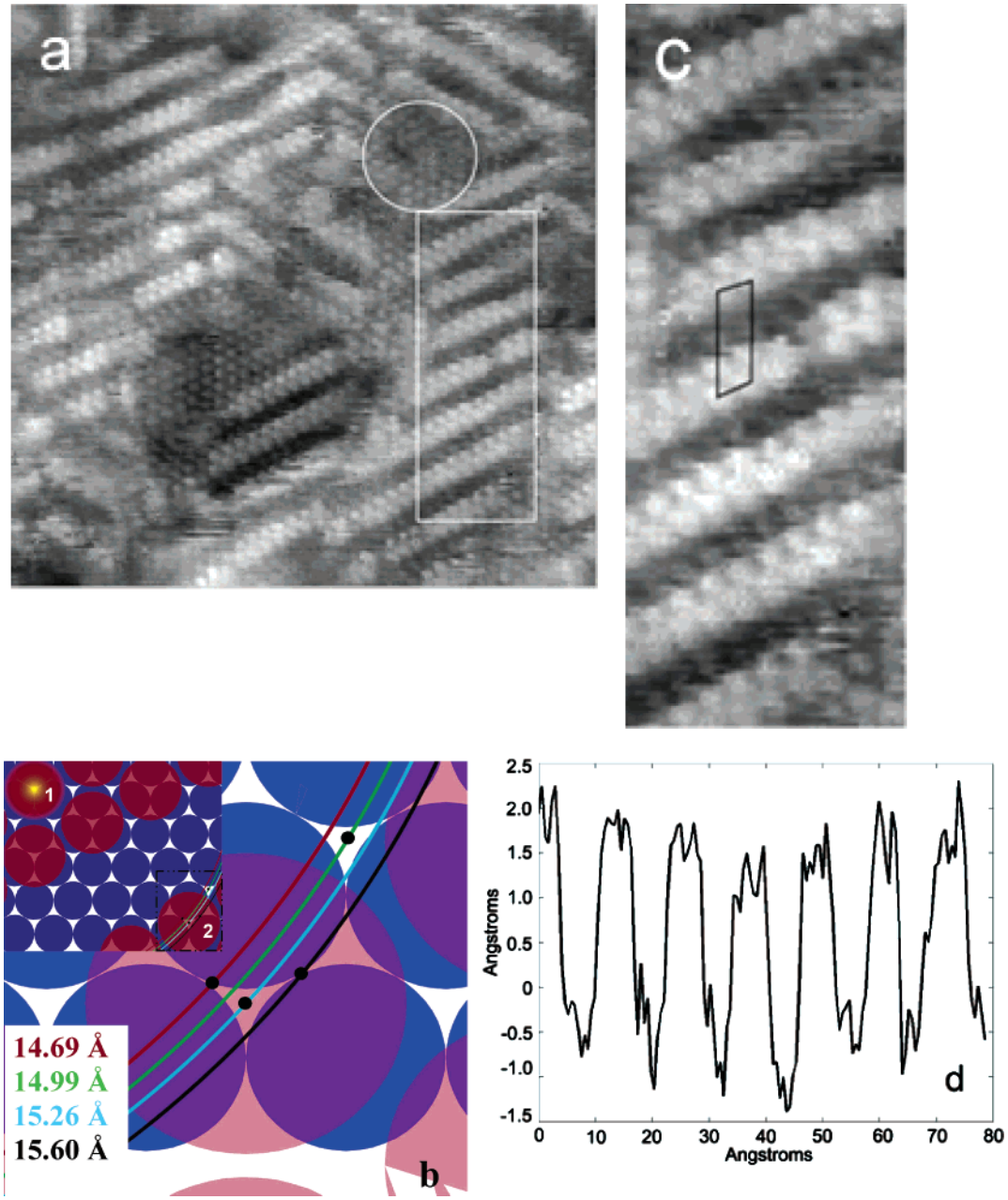

Figure 6. (a) STM image of a 165 Å × 165 Å area of a dodecaneselenolate on Au{111} recorded at sample bias of −1.0 V and 3.0 pA tunneling current, exhibiting the 4.99 Å × 15.60 Å variant of the ($\sqrt{3} \times 3\sqrt{3}$)R30° missing row structure throughout. The white circle shows a section of the film where the linear structures meet, forming an area with a higher molecular density than that in the striped region. (b) Diagram showing the distance between a 3-fold hollow site (molecule 1) and a third nearest neighbor site (molecule 2). The inset is a diagram of the observed structure highlighting the site from which the distances are measured to the potential binding sites. The main body of the diagram shows increasing distances of 14.69, 14.99, 15.26, and 15.60 Å, with black dots indicating potential binding sites at either bridge or 3-fold hollow sites. (c) 88 Å × 40 Å extract from (a) with the ($\sqrt{3} \times 3\sqrt{3}$)R30° unit cell outlined. (d) Line profile across six missing rows with the scan direction parallel to the long axis of the ($\sqrt{3} \times 3\sqrt{3}$)R30° unit cell, showing both the distance between molecules and extra molecules bound ~2 Å lower than the rest of the molecules.

alkanethiolate structures in Au{111} SAMs, from the lying down phase to the fully packed, tilted monolayers with a ($\sqrt{3} \times \sqrt{3}$)R30° unit cell and related superstructures.[5] Of the many different adsorbate features observed in that study we see only the four variants of the ($\sqrt{3} \times 3\sqrt{3}$)R30° unit cell for the alkaneselenolates discussed here. There have been a few instances where we observed the ($\sqrt{3} \times 3\sqrt{3}$)R30° structure with two adjacent rows separated by a binding site registry shift, indicated by a domain boundary, as was previously reported for alkanethiolates.[16,17] However, since we so rarely have observed this structure, we conclude that it is unstable relative to formation of a more closely packed structure. While the close packing arising from filling in the missing row would be expected to result in significant steric repulsion between chains, the gain in energy by increased Au−Se bonds per unit area could provide the necessary driving force for rearrangements to allow the additional molecules. This forcing of the molecules to pack in a tight matrix in turn provides a driving force to relax the domain boundaries separating these row structures, leading to a continuous monolayer. Ideally, a resultant ($\sqrt{3} \times \sqrt{3}$)R30° spacing structure would be expected from such a process. However, we observe a distorted incommensurate structure with spacings of 4.90 and 5.20 Å, in agreement with Samant et al.[37] The differences in the lattice spacings between

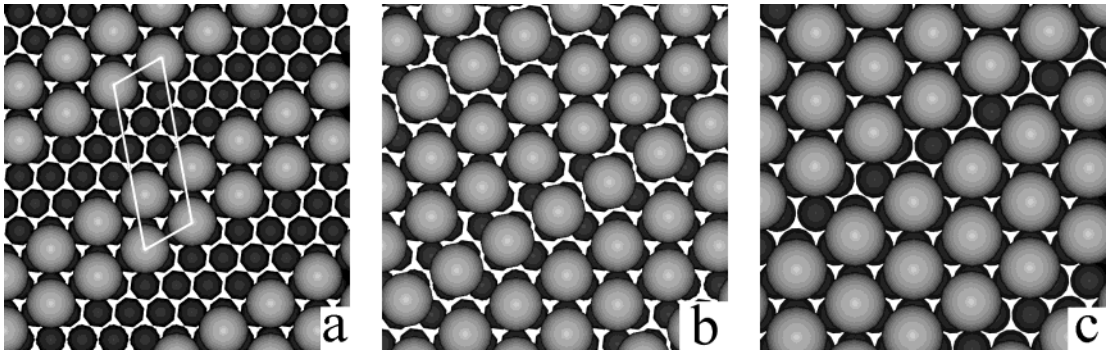

Figure 7. (a) Schematic illustration of a missing row structure with a 4.99 Å × 15.26 Å unit cell spacing. (b) Structure a with the missing rows filled with molecules set on interstitial bridge sites. (c) Structure a with the missing rows filled with molecules set on 3-fold hollow sites. Note that in order to form a full monolayer, structure b would need to undergo both site shifting and compression of the overall structure, while c would need a similar reconstruction following a "zipper-like" registry shift.

the $(\sqrt{3} \times \sqrt{3})$R30° alkanethiolate and the 4.90 Å × 5.20 Å alkaneselenolate unit cells involve headgroup atoms shifting along both cell axes; in the case of 4.90 Å, this shift is a compression, and for 5.20 Å, the shift is an expansion. Assuming that molecules are initially bound to either 3-fold hollow or bridge sites at spacings typical of the $(\sqrt{3} \times \sqrt{3})$R30° and its superlattices and using distances between 3-fold and bridge sites on the unreconstructed Au{111} surface as a guide to minimum energy sites, we infer that the differences in unit cell dimensions are based both on simultaneous headgroup−headgroup, and headgroup−substrate interactions. These headgroup−headgroup interactions result in compression, while the headgroup−substrate interactions will result in expansion, as discussed in further detail below.

The Monolayer Growth Mechanism. The overall growth mechanism of alkaneselenolate SAMs can be developed further by considering recent electrochemical studies that suggest that full monolayer formation takes place in two steps.[32] Coupling this with our STM observations, we propose (1) fast formation of the $(\sqrt{3} \times 3\sqrt{3})$R30° structure followed by (2) slow adsorption with concurrent rearrangement to form the 4.90 Å × 5.20 Å unit cell. Shifting from the row structure to the full monolayer could occur via adsorption at sites between the rows or a surface diffusion process such as Ostwald ripening.[7] Our data suggest that the former plays a larger role than the latter. Taking into account the variability in the $(\sqrt{3} \times 3\sqrt{3})$R30° binding sites of the dense-packed phases, the adsorption sites can be determined. If the unit cell of the missing row formation were of the 14.69 Å variant, all that would be needed for the 4.90 Å spacing is to have an additional molecule bind directly between the existing molecules. Likewise, if there is a 15.60 Å variant, the 5.20 Å spacing would occur. These outcomes are seen in Figure 6a,c, where molecules appear in the missing rows. Since it is likely that chemisorption of molecules are isolated events, there is a statistical distribution of initial binding sites. Once chemisorbed, molecules are able to move and to search out the most energetically favorable locations and conformations.

We checked for the nature of the transformation mechanism(s) using time sequence STM images of incomplete coverage regions on our selenolate SAMs. The results suggest that the $(\sqrt{3} \times 3\sqrt{3})$R30° structure is transformed into a full monolayer through Ostwald ripening in which a domain that is pockmarked with vacancy islands (depressions in Figure 5) anneals to one with fewer vacancies of larger sizes (Figure 1). Image features give clues to the mechanism of this transformation. Differently axially aligned linear missing row structures terminate where they meet at 120° angles typically, but not always, at substrate defect sites. These junctions result in densely packed areas where the rows are no longer distinct, and the molecules are tightly packed, as in Figure 6a. Since it has been proposed that vacancy islands are minimum energy nucleation sites for molecular adsorption,[5,7,8] it follows that molecules will preferentially adsorb at these defects and nucleate the formation of a new surface phase in which the missing row is filled. Figure 7a illustrates a missing row structure with the 4.99 Å × 15.26 Å unit cell spacing indicated. The missing row can be filled in two ways: molecules adsorbing at interstitial bridge sites (Figure 7b) or 3-fold hollow sites (Figure 7c).[67] Once filled, these two structures can further anneal to form the observed monolayer by undergoing compression along one unit cell direction and coordinated expansion along the other (bridge site) or translating entire rows together in a "zipper-like" fashion (3-fold hollow site), followed by a subsequent rearrangement. The latter "zipper" motion removes the domain boundaries via a simple registry shift of the misaligned rows. The net effect of these two types of motion appears to be large-scale surface reconstruction in which a large number of line defects are squeezed out, creating a continuous incommensurate monolayer, and substrate defects collect into a few large areas consisting of voids and islands. Additionally, by reconstructing the monolayer/surface structure, previously unavailable binding sites may be opened and more molecules could bind or move to the defect. At some point the surface becomes saturated with adsorbates, locking in areas composed of missing rows and of the compressed monolayer. Partial remnants of the missing row structure are seen as inclusions in the more compact monolayer. Thus, the ripening process of meeting rows and molecular movements can yield a highly packed monolayer of uniform coverage with little evidence of prior domain structures.

The Role of Headgroup Interactions—Differences Between Se−Se and S−S Interactions. Three main possibilities can be proposed to explain the differences between the multiple selenolate SAM structures and the established $(m\sqrt{3} \times n\sqrt{3})$-R30° unit cell for thiolates: (1) enhanced local shifting of alkaneselenolate molecules between binding sites compared to alkanethiolates, (2) enhanced headgroup−headgroup interactions in alkaneselenolates compared to alkanethiolates, and (3) the larger diameter of Se compared to S. Differences between most of the $(\sqrt{3} \times 3\sqrt{3})$R30° variant structures are small enough to be accounted for by the adsorbate atoms being slightly off the exact binding site, as suggested by Molina and Yourdshahyan,[47,66] or simply by the 0.20 Å difference in the van der Waals diameters between S and Se. However, the alkaneselenolate $(\sqrt{3} \times 3\sqrt{3})$R30° variant with either the 14.69 or 15.60 Å length is not consistent with the influence of the size difference and thus must be explained by shifted binding

sites. Alternatively, the shift of binding sites can be described by having significantly different headgroup environment (substrate or other headgroup) interactions. Since larger shifts in binding sites imply that the molecule is driven to find a deeper energy minimum, this type of shift can be attributed to headgroup−substrate interactions. The binding site shifting argument is augmented by considering the expanded portion of the unit cell of the full monolayer structure, (5.20 Å compared to 4.99 Å). This expansion is a result of switching the binding sites from one site to the next on the Au surface, i.e., from a bridge site to a 3-fold site or vice versa. This headgroup−substrate interaction provides evidence that either the bridge site or 3-fold site is favorable for binding, with the exact location of the molecule being dependent more on the headgroup interactions with other headgroups and the substrate.

An additional headgroup−surface interaction is manifested in the "missing row" formation. The ~2 Å difference in apparent height (Figure 6d) is equivalent to a missing Au substrate atom. The strong interaction of the selenolate group with the gold surface leads to a substantial reconstruction of the surface.

Significant headgroup−headgroup interactions are observed. Defects occurring pairwise in the missing row double layer are visible in Figure 6c just to the right of the box indicating the unit cell. Poirier described a $(\sqrt{3} \times 3\sqrt{3})$R30° structure similar to the feature that we observed, which he called the χ phase, $c(19 \times \sqrt{3})$ on Au{111}, where a close pairing of sulfur headgroups is maintained in a coverage-dependent experiment on decanethiol on Au{111}.[5,8] Additionally, selenolate molecules experience a force that yields a slight compression toward each other in the complete monolayer, as the unit cell is altered compared to the $(\sqrt{3} \times \sqrt{3})$R30° structure observed for thiolates. At a separation of 4.90 Å, there are no open 3-fold, bridge, or atop sites available nearby for binding the molecule; thus, there must be another driving force to compress the headgroup spacings. Whatever the mechanism, this allows the Se−Se spacing to be ~0.1 Å less than observed for thiolates (4.90 Å compared to 4.99 Å). In combination with the headgroup−surface interactions, these headgroup−headgroup interactions help determine the surface morphology of the selenolate adlayer.

Conclusions and Prospects

It has been demonstrated through STM imaging and structural modeling that the packing and arrangement of decaneselenolate and dodecaneselenolate monolayers on Au{111} include two types of structures. We infer from our results for high coverage monolayers that selenolates have multiple binding sites. This interpretation for alkaneselenolates is consistent with both structural variants of the $(\sqrt{3} \times 3\sqrt{3})$R30° unit cell as well as the incommensurate 4.90 Å × 5.20 Å unit cell for the fully packed monolayer.

Surface transformations are observed to occur in the selenolate SAMs where coverages are not complete. Through processes including Ostwald ripening and binding site hopping, the SAMs can undergo transformations to attain more stable configurations where missing row formations meet. This process minimizes surface strain and lattice mismatch energies of adsorbates.

Since these fully packed alkaneselenolate SAMs are coherent and lack apparent domain boundary structures, most of the molecules must be tilted in the same direction. Given that it has recently been demonstrated that crystalline objects can grow in certain predictable orientations given a certain tilt angle of a SAM, having a monolayer with a known uniform tilt may provide a useful template for growth of single-crystal films.[68] While biaxial tilt measurements cannot be addressed using STM, such data can be acquired using oriented single crystals and spectroscopic methods such as infrared spectroscopy, and such measurements are underway in our laboratory.[69]

With these results and the generalization that electronic coupling between molecules is higher when the headgroup is Se rather than S,[33] selenolate SAMs add to the repertoire of structures and materials that can be applied to nanoscale science and technology.

Acknowledgment. The authors would like to thank K. F. Kelly and L. A. Bumm for especially stimulating conversations about the interpretation of our data. Support is gratefully acknowledged from DARPA, NIST, NSF, and ONR.

References and Notes

(1) Bumm, L. A.; Arnold, J. J.; Charles, L. F.; Dunbar, T. D.; Allara, D. L.; Weiss, P. S. *J. Am. Chem. Soc.* **1999**, *121*, 8017−8021.
(2) Yamada, R.; Wano, H.; Uosaki, K. *Langmuir* **2000**, *16*, 5523−5525.
(3) Stranick, S. J.; Parikh, A. N.; Tao, Y. T.; Allara, D. L.; Weiss, P. S. *J. Phys. Chem.* **1994**, *98*, 7636−7646.
(4) Smith, R. K.; Reed, S. M.; Lewis, P. A.; Monnell, J. D.; Clegg, R. S.; Kelly, K. F.; Bumm, L. A.; Hutchison, J. E.; Weiss, P. S. *J. Phys. Chem. B* **2001**, *105*, 1119−1122.
(5) Poirier, G. E. *Langmuir* **1999**, *15*, 1167−1175.
(6) Poirier, G. E. *Chem. Rev.* **1997**, *97*, 1117−1127.
(7) Poirier, G. E. *Langmuir* **1997**, *13*, 2019−2026.
(8) Poirier, G. E.; Pylant, E. D. *Science* **1996**, *272*, 1145−1148.
(9) Poirier, G. E.; Tarlov, M. J. *J. Phys. Chem.* **1995**, *99*, 10966−10970.
(10) Poirier, G. E.; Tarlov, M. J. *Langmuir* **1994**, *10*, 2853−2856.
(11) Persson, B. N. J. *Surf. Sci. Rep.* **1992**, *15*, 1−135.
(12) Lewis, P. A.; Smith, R. K.; Kelly, K. F.; Bumm, L. A.; Reed, S. M.; Clegg, R. S.; Gunderson, J. D.; Hutchison, J. E.; Weiss, P. S. *J. Phys. Chem. B* **2001**, *105*, 10630−10636.
(13) Han, S. W.; Lee, S. J.; Kim, K. *Langmuir* **2001**, *17*, 6981−6987.
(14) Camillone, N.; Eisenberger, P.; Leung, T. Y. B.; Schwartz, P.; Scoles, G.; Poirier, G. E.; Tarlov, M. J. *J. Chem. Phys.* **1994**, *101*, 11031−11036.
(15) Anselmetti, D.; Baratoff, A.; Guntherodt, H. J.; Delamarche, E.; Michel, B.; Gerber, C.; Kang, H.; Wolf, H.; Ringsdorf, H. *Europhys. Lett.* **1994**, *27*, 365−370.
(16) Schonenberger, C.; Jorritsma, J.; Sondag-Huethorst, J. A. M.; Fokkink, L. G. J. *J. Phys. Chem.* **1995**, *99*, 3259−3271.
(17) Schonenberger, C.; Sondag-Heuthorst, J. A. M.; Jorritsma, J.; Fokkink, L. G. J. *Langmuir* **1994**, *10*, 611−614.
(18) Zharnikov, M.; Grunze, M. *J. Phys. Condens. Mater.* **2001**, *13*, 11333−11365.
(19) Zharnikov, M.; Frey, S.; Rong, H.; Yang, Y. J.; Heister, K.; Buck, M.; Grunze, M. *Phys. Chem. Chem. Phys.* **2000**, *2*, 3359−3362.
(20) Frey, S.; Heister, K.; Zharnikov, M.; Grunze, M.; Tamada, K.; Colorado, R. J.; Graupe, M.; Shmakova, O. E.; Lee, T. R. *Isr. J. Chem.* **2000**, *40*, 81−97.
(21) Ulman, A. *An Introduction to Ultrathin Organic Films: Langmuir−Blodgett to Self-Assembly*; Academic Press: New York, 1991.
(22) Ulman, A. *Chem. Rev.* **1996**, *96*, 1533−1554.
(23) Ulman, A. *Thin Films: Self-assembled monolayers of thiols*; Academic Press: San Diego, CA, 1998.
(24) Rong, H. T.; Frey, S.; Yang, Y. J.; Zharnikov, M.; Buck, M.; Wuhn, M.; Woll, C.; Helmchen, G. *Langmuir* **2001**, *17*, 1582−1593.
(25) Henderson, J. I.; Feng, S.; Ferrence, G. M.; Bein, T.; Kubiak, C. P. *Inorg. Chim. Acta* **1996**, *242*, 115−124.
(26) Henderson, J. I.; Feng, S.; Bein, T.; Kubiak, C. P. *Langmuir* **2000**, *16*, 6183−6187.
(27) Hong, S.; Reifenberger, R.; Tian, W.; Datta, S.; Henderson, J.; Kubiak, C. P. *Superlattices Microstruct.* **2000**, *28*, 289−303.
(28) Bain, C. D.; Evall, J.; Whitesides, G. M. *J. Am. Chem. Soc.* **1989**, *111*, 7155−7164.
(29) Huc, V.; Bourgoin, J.-P.; Bureau, C.; Valin, F.; Zalczer, G.; Palacin, S. *J. Phys. Chem. B* **1999**, *103*, 10489−10495.
(30) Nakamura, T.; Kimura, R.; Matsui, F.; Kondoh, H.; Ohta, T.; Sakai, H.; Abe, M.; Matsumoto, M. *Langmuir* **2000**, *16*, 4213−4216.
(31) Nakamura, T.; Yasuda, S.; Miyamae, T.; Nozoye, H.; Kobayashi, N.; Kondoh, H.; Nakai, I.; Ohta, T.; Yoshimura, D.; Matsumoto, M. *J. Am. Chem. Soc.* **2002**, *124*, 12642−12643.
(32) Protsailo, L. V.; Fawcett, W. R.; Russell, D.; Meyer, R. L. *Langmuir* **2002**, *18*, 9342−9349.

(33) Patrone, L.; Palacin, S.; Bourgoin, J. P.; Lagoute, J.; Zambelli, T.; Gauthier, S. *Chem. Phys.* **2002**, *281*, 325−332.
(34) Venkataramanan, M.; Skanth, G.; Bandyopadhyay, K.; Vijayamohanan, K.; Pradeep, T. *J. Colloid Interface Sci.* **1999**, *212*, 553−561.
(35) Bandyopadhyay, K.; Vijayamohanan, K.; Venkataramanan, M.; Pradeep, T. *Langmuir* **1999**, *15*, 5314−5322.
(36) Bandyopadhyay, K.; Vijayamohanan, K. *Langmuir* **1998**, *14*, 625−629.
(37) Samant, M. G.; Brown, C. A.; Gordon, J. G., II *Langmuir* **1992**, *8*, 1615−1618.
(38) Aslam, M.; Bandyopadhyay, K.; Vijayamohanan, K.; Lakshminarayanan, V. *J. Colloid Interface Sci.* **2001**, *234*, 410−417.
(39) Dishner, M. H.; Hemminger, J. C.; Feher, F. J. *Langmuir* **1997**, *13*, 4788−4790.
(40) Lister, T. E.; Stickney, J. L. *J. Phys. Chem.* **1996**, *100*, 19568−19576.
(41) Huang, F. K.; Horton, R. C.; Myles, D. C.; Garrell, R. L. *Langmuir* **1998**, *14*, 4802−4808.
(42) Han, S. W.; Kim, K. *J. Colloid Interface Sci.* **2001**, *240*, 492−497.
(43) Yaliraki, S. N.; Kemp, M.; Ratner, M. A. *J. Am. Chem. Soc.* **1999**, *121*, 3428−3434.
(44) Sorenson, T. A.; Lister, T. E.; Huang, B. M.; Stickney, J. L. *J. Electrochem. Soc.* **1999**, *146*, 1019−1027.
(45) Seminario, J. M.; Zacarias, A. G.; Tour, J. M. *J. Am. Chem. Soc.* **1999**, *121*, 411−416.
(46) Poirier, G. E. *J. Vac. Sci. Technol. B* **1996**, *14*, 1453−1460.
(47) Molina, L. M.; Hammer, B. *Chem. Phys. Lett.* **2002**, *360*, 264−271.
(48) Noh, J.; Hara, M. *Langmuir* **2001**, *17*, 7280−7285.
(49) Dishner, M. H.; Hemminger, J. C.; Feher, F. J. *Langmuir* **1997**, *13*, 2318−2322.
(50) Delamarche, E.; Michel, B.; Gerber, C.; Anselmetti, D.; Guntherodt, H. J.; Wolf, H.; Ringsdorf, H. *Langmuir* **1994**, *10*, 2869−2871.
(51) For clarity, $c(3 \times 2\sqrt{3})$ is synonymous with a hexagonal $(4\sqrt{3} \times 2\sqrt{3})R30°$ structure, both of which are centered superlattices of the $(\sqrt{3} \times \sqrt{3})R30°$ unit cell, which we use as the basis for comparison between thiolate and selenolate monolayers.
(52) Reinerth, W. A.; Tour, J. M. *J. Org. Chem.* **1998**, *63*, 2397−2400.
(53) Gladysz, J. A.; Hornby, J. L.; Garbe, J. E. *J. Org. Chem.* **1978**, *43*, 1204−1208.
(54) Parkinson, B. A.; Ohuchi, F. S.; Ueno, K.; Koma, A. *Appl. Phys. Lett.* **1991**, *58*, 472−474.
(55) Rong, Z. Y.; Kuiper, P. *Phys. Rev. B* **1993**, *48*, 17427−17431.
(56) Terada, S.; Yokoyama, T.; Saito, N.; Okamoto, Y.; Ohta, T. *Surf. Sci.* **1999**, *435*, 657−660.
(57) Sasaki, M.; Yamada, Y.; Ogiwara, Y.; Yagyu, S.; Yamamoto, S. *Phys. Rev. B* **2000**, *61*, 15653−15656.
(58) Novaco, A. D.; McTague, J. P. *Phys. Rev. Lett.* **1977**, *38*, 1286−1289.
(59) Kobayashi, K. *Phys. Rev. B* **1996**, *53*, 11091−11099.
(60) Kobayashi, K. *Phys. Rev. B* **1994**, *50*, 4749−4755.
(61) Harten, U.; Lahee, A. M.; Toennies, J. P.; Woll, C. *Phys. Rev. Lett.* **1985**, *54*, 2619−2622.
(62) Chambliss, D. D.; Wilson, R. J. *J. Vac. Sci. Technol. B* **1991**, *9*, 928−932.
(63) Carter, C. B.; Hwang, R. Q. *Phys. Rev. B* **1995**, *51*, 4730−4733.
(64) Brune, H.; Roder, H.; Borango, C.; Kern, K. *Phys. Rev. B* **1994**, *49*, 2997−3000.
(65) Kluth, G. J.; Carraro, C.; Maboudian, R. *Phys. Rev. B* **1999**, *59*, R10449−R10452.
(66) Yourdshahyan, Y.; Rappe, A. M. *J. Chem. Phys.* **2002**, *117*, 825−833.
(67) For unit cell lengths other than 15.26 Å (as in Figure 6b), the missing rows can be filled in a similar fashion, with similar results.
(68) Aizenberg, J.; Black, A. J.; Whitesides, G. M. *Nature* **1999**, *398*, 495−498.
(69) Preliminary results on polycrystalline Au{111} indicate that the alkyl chains in octadecane selenolate SAMs exhibit average tilt angles of 27° from the surface normal (Dunbar, T. D.; Reinerth, W. A.; Arnold, J. J.; Bumm, L. A.; Weiss, P. S.; Tour, J. M.; Allara. D. L., manuscript in preparation). Earlier work by Samant and co-workers using X-ray diffraction, in contrast, suggests a coherent tilt angle of 15°, see ref 37.